RESEARCH ARTICLE | SEPTEMBER 08 2025

Dynamics of polymer rings: The Rouse ring chain with attractive harmonic potential of spherical symmetry

Nail Fatkullin ; Carlos Mattea ; Kevin Lindt ; Siegfried Stapf ; Margarita Kruteva

J. Chem. Phys. 163, 104901 (2025)
https://doi.org/10.1063/5.0285040

The Journal of Chemical Physics ARTICLE pubs.aip.org/aip/jcp

Dynamics of polymer rings: The Rouse ring chain with attractive harmonic potential of spherical symmetry

Cite as: J. Chem. Phys. 163, 104901 (2025); doi: 10.1063/5.0285040
Submitted: 12 June 2025 • Accepted: 19 August 2025 •
Published Online: 8 September 2025

Nail Fatkullin,[1] Carlos Mattea,[1] Kevin Lindt,[1] Siegfried Stapf,[1] and Margarita Kruteva[2,a)]

AFFILIATIONS

[1] Technische Physik II/Polymerphysik, Technische Universität Ilmenau, D-98684 Ilmenau, Germany
[2] Jülich Centre for Neutron Science (JCNS-1), Forschungszentrum Jülich GmbH, 52428 Jülich, Germany

[a)] Author to whom correspondence should be addressed: m.kruteva@fz-juelich.de

ABSTRACT

The static and dynamic properties of a cyclic Rouse chain modified by the introduction of an effective, spherically symmetric, attracting potential of entropic nature are studied. It is shown that a relatively weak potential can lead to a strong contraction of the polymer chain: the radius of gyration becomes much smaller compared to the size of the free cyclic chain. The pronounced decrease in the terminal relaxation time of cyclic macromolecules in the presence of a harmonic potential compared to the Rouse relaxation time leads to a lengthening of the time interval for the transition to the normal, i.e., the Fickian, diffusion regime, generating a quasi-plateau at increasing molecular mass for the time dependence of segmental mean squared displacement.

I. INTRODUCTION

In recent years, interest in polymeric systems containing ring macromolecules has increased markedly.[1–16] As shown, e.g., by rheology and neutron scattering experiments, the absence of end segments in cyclic macromolecules leads to serious differences in their conformations and dynamics in comparison with linear analogs of equal molecular mass. It also has an essential impact on biology: DNA in the genome forms cyclic structures that are much more compact than their linear analogs. In particular, linear macromolecules in melts have conformations that are, with sufficient accuracy, close to ideal Gaussian conformation,[17–22] i.e., without intra-chain excluded volume interactions. The mean square of their radius of gyration depends linearly on the molecular weight $R^2_{g,lin} = \frac{Nb^2}{6}$, where b is the length of a Kuhn segment and N is the number of Kuhn segments per macromolecule. In the case of melts of cyclic macromolecules, the absence of end segments generates entropic interactions preventing mutual penetration of macromolecules into each other, which leads to a significant weakening of the molecular-mass dependence of the mean squared radius of gyration $R^2_{g,ring} \propto b^2 N^{\nu}$ with $\nu \approx \frac{2}{3}$ as has been shown by simulations.[6,7] In other words, these additional topological constraints appear to be similar to effective intramolecular attractive interactions related to the center of mass of the ring, leading to more compact, globular conformations. The latter circumstance makes the analytical description of the structure and dynamics of cyclic macromolecules more complicated compared to their linear analogs, since even at the level of intramolecular interactions, the non-Gaussian distribution of conformations gives rise to nonlinear equations of motion. It should also be noted that the methods used in experimental studies of ring macromolecules are the same as those used for their linear analogs.[17–22] The main difference from an experimental point of view lies in the synthesis and preparation of well-characterized systems of ring macromolecules with large molecular weights.

In the theory of dynamic properties of linear polymers, the Rouse model plays an important supporting role because it is exactly solvable.[17–22] Although it does not include entanglement effects, it can be at least phenomenologically modified, for example, by constraints for chain motions inside the tube at times smaller than the terminal relaxation time, as in the reptation tube model, to apply it satisfactorily even for highly entangled systems.

For the case of ring polymer melts, the Rouse model can be applied directly using appropriate boundary conditions for the ends of linear polymer chains.[16] In this case, ring macromolecules have a conformational distribution corresponding to a freely connected ring whose characteristic size is only $\sqrt{2}$ times smaller than the size of linear chains containing the same number of Kuhn segments, and the mean squared radius of gyration scales as $R^2_{g,ring} = \frac{Nb^2}{12}$. In other words, this simplified approach does not consider the effects of contraction of polymer rings in melts associated with the above-mentioned topological constraints on mutual penetrations.

This contraction effect can be considered by introducing a harmonic potential of spherical symmetry, which attracts any of the ring segments to the ring center of mass with a constant strength as a parameter. After this modification, the Rouse model is still exactly analytically tractable and can play the role of a reference model for the dynamical properties of polymer rings. As far as we know, this model, although amenable to an exact solution, has not yet been described in the literature. However, a similar model containing a modification of the Rouse model with an axially symmetric harmonic two-dimensional potential to study various aspects of the reptation model in linear polymers has been considered.[23,24] A recent work discusses the dynamics of generalized Rouse linear chains in an external harmonic potential of spherical symmetry, demonstrating that the external potential induces additional correlations between monomers, affecting the nature of friction between polymer segments and their surroundings through the influence of memory functions in the generalized Langevin equation.[25] In this paper, we present the Rouse model modified by an effective three-dimensional attractive internal harmonic potential to describe the dynamics of a ring polymer, which in this context is of independent scientific interest.

II. THEORY

Let us consider a polymer ring consisting of $N \gg 1$ statistical Kuhn segments. Then the effective Hamiltonian, more precisely the effective intramolecular potential energy, is defined by the following expression:

$$H = \frac{3k_BT}{2}\sum_n \left(\frac{1}{b^2}\left(\frac{\partial \vec{r}_n}{\partial n}\right)^2 + \frac{(\vec{r}_n - \vec{r}_{cm})^2}{\tilde{R}^2}\right), \tag{1}$$

where $\tilde{R}$ is a parameter of the potential. The first term on the right-hand side of Eq. (1) describes the conventional, effectively intramolecular entropic interactions of an ideal polymer chain,[17–22] while the second term, which has the structure of a harmonic potential, is related to the effects of entropic contraction of the polymer chain caused by topological constraints of mutual penetration of cyclic macromolecules into each other. Note also that because $N \gg 1$, the continuous limit and summation over n is equivalent to integration over n. The parameter of the potential $\tilde{R}$ is defined in a way such that, in the case of an isolated segment, its mean squared distance from the minimum of the potential is equal to

$$\langle r^2 \rangle = \tilde{R}^2, \tag{2}$$

where $\tilde{R}$ is the characteristic radius of the harmonic potential. The larger this quantity, the weaker the potential.

The equation of motion for a Rouse ring is as follows:

$$\zeta \frac{\partial \vec{r}_n(t)}{\partial n} = \frac{3k_BT}{b^2}\frac{\partial^2}{\partial n^2}\vec{r}_n(t) - \frac{3k_BT}{\tilde{R}^2}(\vec{r}_n(t) - \vec{r}_{cm}(t)) + \vec{f}^L_n(t), \tag{3}$$

where ζ is the segmental friction coefficient, $\vec{f}^L_n(t)$ is the stochastic Langevin force acting on segment with number n at time moment t, $\vec{r}_{cm}(t) = \frac{1}{N}\sum_n \vec{r}_n(t)$ is the position vector of the center of mass of the considered polymer ring at time moment t, $\vec{r}_n(t)$ is the position vector of the segment with number n at time moment t, and k_BT is the Boltzmann constant multiplied by the absolute temperature.

The ring architecture of the polymer chain is taken into account by means of the following boundary conditions:

$$\vec{r}_0(t) \equiv \vec{r}_N(t). \tag{4}$$

These boundary conditions lead to the following Fourier decomposition:

$$\vec{r}_n(t) = \vec{X}_0(t) + \sum_{p=1}^{N/2}\left(2\vec{X}_p(t)\cos\left(\frac{2\pi}{N}pn\right) + 2\vec{Y}_p(t)\sin\left(\frac{2\pi}{N}pn\right)\right). \tag{5}$$

The normal relaxation Rouse modes of the ring macromolecule can be calculated from Eq. (5) by the inverse Fourier transform,

$$\begin{aligned}\vec{X}_p(t) &= \frac{1}{N}\int_0^N \vec{r}_n(t)\cos\left(\frac{2\pi}{N}pn\right)dn,\\ \vec{Y}_p(t) &= \frac{1}{N}\int_0^N \vec{r}_n(t)\sin\left(\frac{2\pi}{N}pn\right)dn.\end{aligned} \tag{6}$$

By substituting Eq. (6) into Eq. (1), we express the Hamiltonian through the normal Rouse modes of the ring macromolecule,

$$H = \frac{3k_BT}{2}\sum_{p=1}^{N/2}\left\{\frac{8\pi^2}{Nb^2}p^2 + \frac{2N}{\tilde{R}^2}\right\}\left(\vec{X}^2_p(t) + \vec{Y}^2_p(t)\right). \tag{7}$$

Assuming the different normal modes fluctuate independently of each other and have a normal Gaussian distribution, we obtain the following relation for their mean-squared values:

$$\frac{1}{\langle \vec{X}^2_p\rangle_{eq}} = \frac{1}{\langle \vec{Y}^2_p\rangle_{eq}} = \left\{\frac{8\pi^2p^2}{Nb^2} + \frac{2N}{\tilde{R}^2}\right\}. \tag{8}$$

Furthermore, from Eqs. (5) and (8), considering the orthogonality of different normal modes, the following expression for the mean squared radius of gyration of the ring macromolecule is obtained:

$$\begin{aligned}R^2_g &\equiv \frac{1}{N}\int_0^N \left\langle (\vec{r}_n(t)) - \vec{X}_0(t)^2\right\rangle = 2\sum_p\left\{\langle \vec{X}^2_p\rangle_{eq} + \langle \vec{Y}^2_p\rangle_{eq}\right\}\\ &= 2\sum_p\left\{\frac{1}{\frac{8\pi^2p^2}{Nb^2} + \frac{2N}{\tilde{R}^2}} + \frac{1}{\frac{8\pi^2p^2}{Nb^2} + \frac{2N}{\tilde{R}^2}}\right\} = 2\sum_{p=1}^{N/2}\frac{1}{\frac{4\pi^2p^2}{Nb^2} + \frac{N}{\tilde{R}^2}}.\end{aligned} \tag{9}$$

For a very weak harmonic potential, $\frac{N^2b^2}{4\pi^2} \ll \tilde{R}^2$, the polymer ring has an ideal, not perturbed, size,[17]

$$R^2_{g,ideal} = \frac{Nb^2}{12}. \tag{10}$$

For large Rouse rings, one observes a globular state,

$$R_g^2 = 2\sum_{p=1}^{N/2} \frac{1}{\frac{4\pi^2 p^2}{Nb^2} + \frac{N}{\tilde{R}^2}} \approx 2\int_1^{N/2} \frac{dp}{\frac{4\pi^2 p^2}{Nb^2} + \frac{N}{\tilde{R}^2}}$$
$$= \frac{\tilde{R}b}{\pi}\left(\arctan\left(\frac{\pi\tilde{R}}{b}\right) - \arctan\left(\frac{2\pi\tilde{R}}{Nb}\right)\right) = \begin{cases} \frac{1}{2}\tilde{R}b \text{ if } \frac{Nb}{2\pi} \gg \tilde{R} \gg \frac{b}{\pi}, \\ \tilde{R}^2 \text{ if } \tilde{R} \ll \frac{b}{\pi}, \end{cases} \tag{11}$$

where the approximation $\arctan(x) = \begin{cases} x & \text{if } x \ll 1, \\ \pi/2 & \text{if } x \gg 1 \end{cases}$ for an infinitely large ring $N \gg 1$ was used.

The limit $\tilde{R} \ll \frac{b}{\pi}$ has mainly academic interest. For the interesting case $\frac{Nb}{2\pi} \gg \tilde{R} \gg \frac{b}{\pi}$, one finds that $R_g^2 = \frac{1}{2}\tilde{R}b \ll \tilde{R}^2$. Recall that $\tilde{R}$ is the inverse measure of the strength of the harmonic potential and equal to the typical distance at which a potentially isolated polymer segment will be separated from the center; see Eq. (2). The relation $R_g = \sqrt{\frac{\tilde{R}b}{2}} \ll \tilde{R}$ indicates that the ring size is much smaller due to the linear connectivity of joined segments. This effect is directly related to the linearly coupled structure of the polymer ring and reflects the fact that there are neighboring segments in close proximity to any segment, resulting in an enhanced attraction by the center of the potential. It is relevant to point out here that despite the constraint $\frac{Nb}{2\pi} \gg \tilde{R}$, the harmonic potential may in fact remain weak because $N \gg 1$.

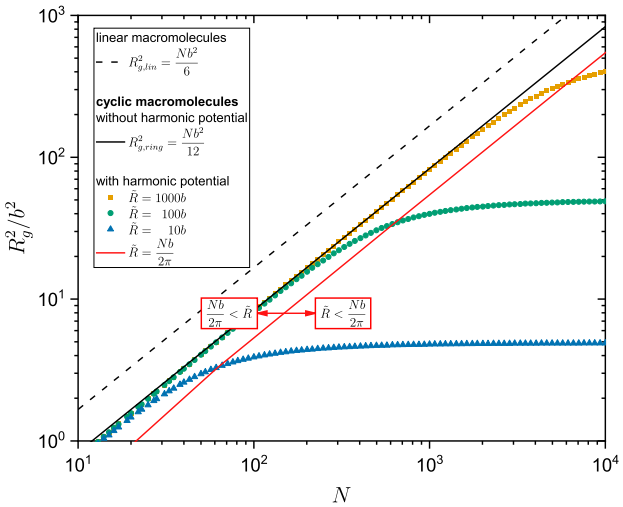

FIG. 1. Dependence of the mean squared radius of gyration R_g^2 of cyclic macromolecules calculated from Eq. (9) and normalized by b^2, experiencing a harmonic potential with characteristic radius $\tilde{R}$ expressed in terms of the number of Kuhn segments N. For a very weak harmonic potential, $\tilde{R} \gg \frac{Nb}{2\pi}$, the mean squared radius of gyration follows the linear dependence on N expected for cyclic macromolecules in the absence of a harmonic potential, $R^2_{g,ring} = \frac{Nb^2}{12}$. For substantially strong potentials, $\frac{Nb}{2\pi} \gg \tilde{R}$, the mean squared radius of gyration approaches a constant value $R_g^2 = \frac{\tilde{R}b}{2}$, as shown in Eq. (11). For comparison, the linear dependence on N for linear macromolecules is also shown.

Figure 1 illustrates Eq. (9), which describes the dependence of the mean squared radius of gyration of the macromolecule on the number of Kuhn segments N for a few characteristic radii $\tilde{R}$ of the harmonic potential. The linear dependence on N for a very weak harmonic potential and the approach to $\frac{1}{2}\tilde{R}b$ for large N are clearly visible.

Expressions for the decay rates of the normal modes, i.e., the inverse relaxation times, can be obtained by differentiating Eq. (5) in time using the equation of motion (3). The result is as follows:

$$\frac{1}{\tau_p} = \frac{4}{\tau_s}\left\{\left(\frac{p}{N}\right)^2 + \frac{1}{4\pi^2}\frac{b^2}{\tilde{R}^2}\right\} = \frac{1}{2\pi^2\tau_s N}\frac{b^2}{\langle \vec{X}_p^2 \rangle} = \frac{1}{2\pi^2\tau_s N}\frac{b^2}{\langle \vec{Y}_p^2 \rangle} \tag{12}$$

with the segmental relaxation time $\tau_s = \frac{\zeta b^2}{3\pi^2 k_B T}$.

Note that the relaxation times of the long-wave Rouse modes with $p \ll \frac{1}{2\pi}\frac{bN}{\tilde{R}} = \frac{1}{4\pi}\frac{b^2 N}{R_g^2}$ cease to depend on the mode number, as shown in Fig. 2. Instead, they depend mainly on the parameter of the harmonic potential $\tilde{R}$.

The quantity $d_{ef} \equiv 2R_g$ can be considered as the effective diameter of the globule. In addition, the value $n_b \equiv \frac{d_{ef}^2}{2b^2}$ turns out to be of the order of the number of Kuhn segments in a section of a macromolecule with linear dimensions of the order of the effective diameter d_{ef} [see also Eq. (25), which shows why it is convenient to include the factor 1/2 in the definition of the number of polymer segments per blob]. Under the influence of an effective spherical potential, the cyclic macromolecules appear to be rolled up into a globule consisting of $N_b = \frac{N}{n_b}$ blobs, each of which contains n_b Kuhn segments.

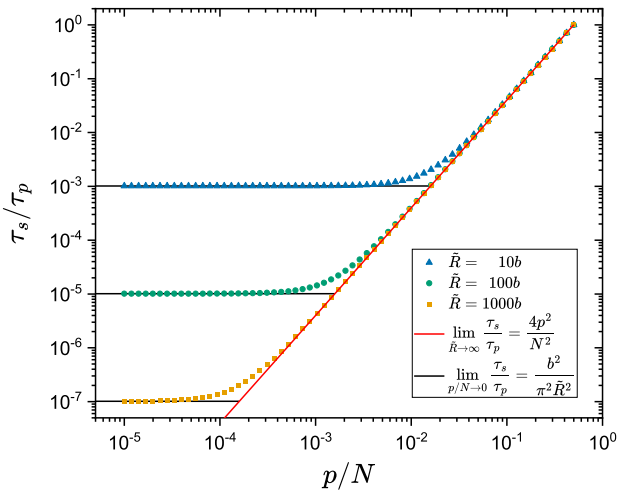

FIG. 2. Dependence of the relaxation time ratio τ_s/τ_p on the mode number $p = 1 \ldots N/2$, normalized by the number of Kuhn segments N, and on the characteristic radius $\tilde{R}$ of the harmonic potential, as described by Eq. (12). The presence of an attractive harmonic potential ($\tilde{R} \ll \infty$) introduces a mode-independent contribution to the Rouse relaxation time, which dominates for $\frac{p}{N} \ll \frac{b}{2\pi\tilde{R}}$.

The mean squared displacement (MSD) of ring segments can be derived from Eq. (5),

$$\left\langle (\vec{r}_n(t) - \vec{r}_n(0))^2 \right\rangle = \left\langle \left(\vec{X}_0(t) - \vec{X}_0(0)\right)^2 \right\rangle + 4\sum_{p=1}^{N/2} \left[\left\langle \vec{X}_p^2 \right\rangle + \left\langle \vec{Y}_p^2 \right\rangle\right] \left(1 - \exp\left\{-\frac{t}{\tau_p}\right\}\right). \quad (13)$$

The first contribution on the right-hand part of Eq. (13) relates to the mean squared displacement of the center of mass, whereas the second part, i.e., the sum over the normal modes $p = 1 \ldots N/2$, describes the motion in the coordinate system connected with this center of mass.

For times $\tau_s \ll t \ll \bar{\tau}_1 \equiv 4\pi^2 \frac{R_g^4}{b^4}\tau_s$, the second term in the right-hand part of Eq. (13) dominates, and anomalous Rouse diffusion is observed,

$$\left\langle (\vec{r}_n(t) - \vec{r}_n(0))^2 \right\rangle \approx 4\sum_{p=1}^{N/2} \left[\left\langle \vec{X}_p^2 \right\rangle + \left\langle \vec{Y}_p^2 \right\rangle\right] \left(1 - \exp\left\{-\frac{t}{\tau_p}\right\}\right) = 8\sum_{p=1}^{N/2} \left\langle \vec{X}_p^2 \right\rangle \left(1 - \exp\left\{-\frac{t}{\tau_p}\right\}\right) \approx \frac{2b^2}{\pi^{3/2}} \left(\frac{t}{\tau_s}\right)^{1/2}. \quad (14)$$

For longer times $\bar{\tau}_1 = 4\pi^2 \frac{R_g^4}{b^4}\tau_S \ll t \ll \bar{\tau}_1^* = \pi^2 \frac{R_g^2 N}{b^2}\tau_s$, the same term still dominates, but the time dependence disappears and a quasi-plateau is reached,

$$\left\langle (\vec{r}_n(t) - \vec{r}_n(0))^2 \right\rangle \approx 4 \sum_{p=1\ldots N/2} \left[\left\langle \vec{X}_p^2 \right\rangle + \left\langle \vec{Y}_p^2 \right\rangle\right] = 2R_g^2. \quad (15)$$

Only for longer times $t \gg \bar{\tau}_1^* = \pi^2 \frac{R_g^2 N}{b^2}\tau_s$, the first term on the right-hand part of Eq. (13), describing normal diffusion of the ring's center of mass, starts to dominate,

$$\left\langle (\vec{r}_n(t) - \vec{r}_n(0))^2 \right\rangle \approx \left\langle \left(\vec{X}_0(t) - \vec{X}_0(0)\right)^2 \right\rangle = \frac{6}{3\pi^2} \frac{b^2}{N} \frac{t}{\tau_s}. \quad (16)$$

Figure 3 illustrates the time-evolution of the mean squared displacement described by Eq. (13) in combination with Eqs. (9), (12), and (16) for different potential radii $\tilde{R}$ and number of Kuhn segments N. The prominent feature visible is the region of constant values, which emerges for a sufficiently strong potential [Fig. 3(a)] and grows with the size of the macromolecules [Fig. 3(b)].

The incoherent dynamical structure factor of ring macromolecules, which is relevant for experiments such as neutron scattering, is given by the following relation:

$$S^{incoh}(k;t) \equiv \frac{1}{N}\sum_n \left\langle \exp\left\{i\vec{k}(\vec{r}_n(t) - \vec{r}_n(0))\right\}\right\rangle = \frac{1}{N}\sum_n \left\langle \exp\left\{-\frac{1}{6}k^2\left\langle (\vec{r}_n(t) - \vec{r}_n(0))^2\right\rangle\right\}\right\rangle. \quad (17)$$

While the coherent dynamical structure factor is

$$S^{\mathrm{coh}}(k;t) \equiv \frac{1}{N}\sum_{n,m} \left\langle \exp\left\{i\vec{k}(\vec{r}_n(t) - \vec{r}_m(0))\right\}\right\rangle = \frac{1}{N}\sum_{n,m} \left\langle \exp\left\{-\frac{1}{6}k^2\left\langle (\vec{r}_n(t) - \vec{r}_m(0))^2\right\rangle\right\}\right\rangle = \frac{1}{N}\sum_{n,m} \varphi_{nm}(k,t) \quad (18)$$

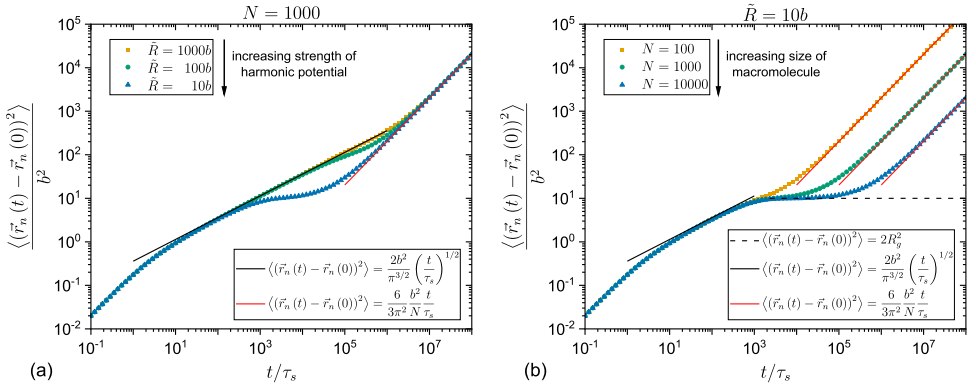

FIG. 3. Illustration of the time-evolution of the mean squared displacement of cyclic macromolecules with harmonic potential in dependence of the characteristic potential radius $\tilde{R}$ and the size of the macromolecule expressed by the number of Kuhn segments N. In the limits $\tau_s \ll t \ll \bar{\tau}_1$ and $t \gg \bar{\tau}_1^*$, the mean squared displacement follows a square-root and linear time dependence described in Eqs. (14) and (16), respectively. Decreasing the characteristic radius of the potential, i.e., increasing its strength, for macromolecules with a fixed number of Kuhn segments results in the formation of a quasi-plateau (a). This range of a time-independent mean squared displacement becomes more pronounced the larger the macromolecules for a fixed potential radius and approaches $2R_g^2 = \tilde{R}b$ if $\frac{Nb}{2\pi} \gg \tilde{R} \gg \frac{b}{\pi}$ (b). The time-evolution is expressed in terms of τ_s, and the mean squared displacement is normalized by the squared length b^2 of a Kuhn segment. The following equation was used to calculate the MSD: $\left\langle (\vec{r}_n(t) - \vec{r}_n(0))^2 \right\rangle = \frac{6}{3\pi^2}\frac{b^2}{N}\frac{t}{\tau_s} + 4\sum_{p=1}^{N/2}\left(\frac{4\pi^2 p^2}{Nb^2} + \frac{N}{\tilde{R}^2}\right)^{-1}\left(1 - \exp\left(-\left(\left(\frac{2p}{N}\right)^2 + \left(\frac{b}{\pi\tilde{R}}\right)^2\right)\frac{t}{\tau_s}\right)\right)$.

with

$$\varphi_{nm}(k,t) \equiv \left\langle \exp\left\{ i\vec{k}(\vec{r}_n(t) - \vec{r}_m(0)) \right\} \right\rangle = \exp\left\{ -\frac{1}{6}k^2 \left\langle \left(\vec{X}_0(t) - \vec{X}_0(0)\right)^2 \right\rangle + 8\sum_{p=1}^{N/2} \left\langle \vec{X}_p^2 \right\rangle \left(1 - \exp\left\{ -\frac{t}{\tau_p} \right\} \cos\left(\frac{2\pi p}{N}(n-m) \right) \right) \right\}. \tag{19}$$

At $t = 0$, Eq. (17) coincides with the so-called static structure factor,

$$g(k) = S^{coh}(k; t=0) = \frac{1}{N}\sum_{n,m} \left\langle \exp\left\{ -\frac{1}{6}k^2 \left\langle (\vec{r}_n(0) - \vec{r}_m(0))^2 \right\rangle \right\} \right\rangle = \frac{1}{N}\sum_{n,m} \varphi_{nm}(k, t=0). \tag{20}$$

The following symmetry applies to ring macromolecules:

$$\varphi_{nm}(k,t) = \varphi_{0n-m}(k,t) = \varphi_{0m-n}(k,t) = \varphi_{mn}(k,t). \tag{21}$$

The latter relationship allows us to rewrite the static structure factor as follows:

$$g(k) = \sum_{m=-N/2}^{N/2} \left\langle \exp\left\{ -\frac{1}{6}k^2 \left\langle (\vec{r}_m(0) - \vec{r}_0(0))^2 \right\rangle \right\} \right\rangle. \tag{22}$$

Using expressions (5) and (8) and the orthogonality of Rouse normal modes, the following relationship can be obtained after calculations:

$$\left\langle (\vec{r}_n(0) - \vec{r}_m(0))^2 \right\rangle = \frac{2Nb^2}{\pi^2} \sum_{p=1}^{N/2} \frac{\sin^2\left(\frac{\pi p(n-m)}{N} \right)}{p^2 + \frac{N^2 b^2}{4\pi^2 \tilde{R}^2}}. \tag{23}$$

If $\frac{Nb}{2\pi} \gg \tilde{R} \gg \frac{b}{\pi}$ and $|n-m| < \frac{N}{2}$, we can approximate summation in relation (23) by integration,

$$\begin{aligned} \left\langle (\vec{r}_n(0) - \vec{r}_m(0))^2 \right\rangle &= \frac{2Nb^2}{\pi^2} \sum_{p=1}^{N/2} \frac{\sin^2\left(\frac{\pi p(n-m)}{N} \right)}{p^2 + \frac{N^2 b^2}{4\pi^2 \tilde{R}^2}} \\ &\approx \frac{2Nb^2}{\pi^2} \int_0^\infty dp \frac{\sin^2\left(\frac{\pi p(n-m)}{N} \right)}{p^2 + \frac{N^2 b^2}{4\pi^2 \tilde{R}^2}} \\ &= \tilde{R}b\left(1 - \exp\left(-\frac{|n-m|b}{\tilde{R}} \right) \right) \\ &= 2\tilde{R}_g^2 \left(1 - \exp\left(-\frac{|n-m|b^2}{2R_g^2} \right) \right). \end{aligned} \tag{24}$$

This expression shows that

$$\left\langle (\vec{r}_n(0) - \vec{r}_m(0))^2 \right\rangle = \begin{cases} |n-m|b^2 & \text{if } |n-m| \ll 2R_g^2/b^2 = d_{ef}^2/2b^2 \equiv n_b, \\ 2\tilde{R}_g^2 & \text{if } |n-m| \gg n_b. \end{cases} \tag{25}$$

Equation (25) again shows that the influence of an effective spherically symmetric internal potential leads to the folding of the ideal conformation by breaking the cyclic macromolecule into $N_b = \frac{N}{n_b}$ blobs containing n_b Kuhn segments. The conformation of each blob is close to that of an ideal macromolecule, and the blobs themselves are randomly distributed around the center of the entire cyclic macromolecule. If we simplify this picture to the extreme, assuming that the conformation of the blobs is strictly ideal and that the mutual distribution of the blobs is completely uncorrelated within the globule, mathematically this is equivalent to replacing strict inequalities $\ll$ and $\gg$ with $\leq$ and $\geq$; then Eq. (22) for the static structure factor can be calculated exactly,

$$g(k) = (N - 2n_b)\exp\left(-\frac{k^2 R_g^2}{6} \right) + \frac{12}{k^2 b^2}\left(1 - \exp\left\{ -\frac{k^2 R_g^2}{3} \right\} \right). \tag{26}$$

III. DISCUSSION

It is instructive to discuss the density distribution of the segments belonging to the ring at position $\vec{r}$ with respect to its center of mass,

$$\tilde{\rho}_s(\vec{r}) \equiv \sum_n \left\langle \delta(\vec{r} - \vec{r}_n + \vec{r}_{cm}) \right\rangle. \tag{27}$$

Since in a ring macromolecule, all segments are equivalent to each other, and in our simplified model, the distribution of normal Rouse modes is assumed to be Gaussian, this value is equal to

$$\tilde{\rho}_s(\vec{r}) = \frac{N}{\left(\frac{2\pi}{3}R_g^2\right)^{3/2}} \exp\left(-\frac{3}{2}\frac{\vec{r}^{\,2}}{R_g^2} \right). \tag{28}$$

In particular, the maximum value for the concentration of own segments is reached at the position of the ring center of mass,

$$\tilde{\rho}_s(\vec{r} = 0) = \frac{N}{\left(\frac{2\pi}{3}R_g^2\right)^{3/2}}. \tag{29}$$

If a polymeric macromolecule containing N Kuhn segments is contracted to a spherical globule with the radius $\tilde{R}_{sf}$ such that this globule contains only its own segments, their concentration will be equal to the average concentration of polymeric segments in the melt ρ_s,

$$\rho_s = \frac{N}{\frac{4\pi}{3}\tilde{R}_{sf}^3}. \tag{30}$$

By dividing Eq. (29) by Eq. (30), we obtain a value indicating the fraction of the globule's own segments' density relative to the density of all segments at the position of the globule's center of mass,

$$\frac{\tilde{\rho}_s(0)}{\rho_s} = \sqrt{\frac{6}{\pi}}\left(\frac{\tilde{R}_{sf}}{R_g} \right)^3. \tag{31}$$

For example, $\frac{\tilde{\rho}_s(0)}{\rho_s} \approx 0.432$ for polyethylene oxide (PEO) rings with a molecular mass $M = 96$ kDa, where $R_g \approx 49.5$Å [from small-angle neutron scattering (SANS) experiments][10,11], $N \approx 701$, $Z = 41$, and $\tilde{R}_{sf} = \left[\frac{3}{4\pi}\frac{m_p}{\rho}M \right]^{1/3} \approx 33.6$Å,[26] with the proton mass m_p and the density of a PEO melt $\rho \approx 1.08$ g/cm^3.[27] This result is numerically very close to recent computer simulations,[14] and Eq. (28) at least qualitatively coincides with Fig. 3(b) from that work. In particular, the intramolecular monomer density as a function of distance from the center-of-mass of a ring scaled by its radius-of-gyration R_g for different ring molecular weights N_b apparently has a Gaussian shape with the maximum at the center-of-mass. The normalized

maximum value for the monomer density at the center-of-mass is about 0.38–0.39, which is in reasonable agreement with the value for $\frac{\tilde{\rho}_s(0)}{\rho_s} \approx 0.432$ for polyethylene oxide (PEO) rings calculated above.

In this very simplified approach, the characteristic radius $\tilde{R}$ of the harmonic potential is a fitting quantity. Computer simulations show that for $N \gg 1$, the value of $\tilde{\rho}_s(0)$ ceases to depend on N and becomes equal to some constant fraction of ρ_s.[14] Using Eq. (29) and recalling that in the case of interest $R_g^2 = \frac{1}{2}\tilde{R}b$, we obtain that the required relation between $\tilde{\rho}_s(0)$ and ρ_s is achieved if the parameter $\tilde{R}^2$ has the following structure:

$$\tilde{R}^2 = \frac{\beta}{b^2}\left(\frac{N}{\rho_s}\right)^{4/3}, \tag{32}$$

where β is a dimensionless numerical coefficient of order 1, possibly reflecting details of the chemical structure of the Kuhn segment. The latter corresponds to the following harmonic potential:

$$U\{\vec{r}_n\} = \frac{3k_BT}{2}\sum_n \frac{(\vec{r}_n - \vec{r}_{cm})^2}{\tilde{R}^2} = \frac{3k_BT}{2}\sum_n \frac{\rho_s^{4/3}b^2}{\beta N^{4/3}}(\vec{r}_n - \vec{r}_{cm})^2. \tag{33}$$

Note that this potential is actually very weak because $N \gg 1$. Using Eqs. (29) and (32), we obtain

$$\tilde{\rho}_s(0) = \left(\frac{3}{\pi\sqrt{\beta}}\right)^{3/2}\rho_s. \tag{34}$$

The concentration of the intrinsic ring segments inside the globule becomes comparable to the total concentration of Kuhn segments in the melt $\tilde{\rho}_s \propto \frac{N}{R_g^3} \propto \rho_s$ and does not depend on N. For an infinitely large Gaussian ring, the concentration of self-segments is much smaller and depends on N in the form of $N^{-1/2}$. A qualitatively similar behavior has been observed in recent computer simulations.[4,5] Using the ratio $\frac{\tilde{\rho}_s(0)}{\rho_s} \approx 0.432$, which was determined for melts of PEO rings, we obtain $\beta = \left(\frac{3}{\pi}\right)^2\left[\frac{\rho_s}{\tilde{\rho}_s(0)}\right]^{4/3} \approx 2.79$, which reasonably satisfies the property of a coefficient of order 1.

Instead of the concentration of Kuhn segments ρ_s in the melt, the so-called packing length of the melt p_l is used hereafter. Both these quantities are related by definition by the following relation:[27]

$$\frac{1}{p_l} \equiv \rho_s b^2. \tag{35}$$

From Eqs. (11) and (32), it follows that $\tilde{R}^2 = \beta N^{4/3}\left(\frac{p_l}{b}\right)^{4/3}b^2$ and $R_g^2 = \frac{\beta^{1/2}}{2}N^{2/3}\left(\frac{p_l}{b}\right)^{2/3}b^2$. Note that the characteristic ratio $\frac{p_l}{b}$ also appears in the expression for the number between neighboring entanglements in polymer melts, $N_e \approx \left(\frac{21.3p_l}{b}\right)^2$, which can be easily verified using published experimental data.[27]

Figure 4 illustrates the dependence of the mean square of the radius of gyration on the molecular mass of a cyclic macromolecule with the potential described in Eq. (33), i.e., Eq. (9), but now taking into account the relation between the radius $\tilde{R}$ of the potential and the number of Kuhn segments N, as described in Eq. (32). As a result, the mean squared radius of gyration no longer reaches a constant value at large N but rather approaches a $N^{2/3}$ dependence, as observed in computer simulations.[6,7] Note that the $N^{2/3}$ dependence (globule with the fractal dimension $\nu = 1/3$) has not been observed experimentally,[9,11] which may be related to the broad transition to the asymptotic behavior, which is not reachable for the synthesized rings (Fig. 4).

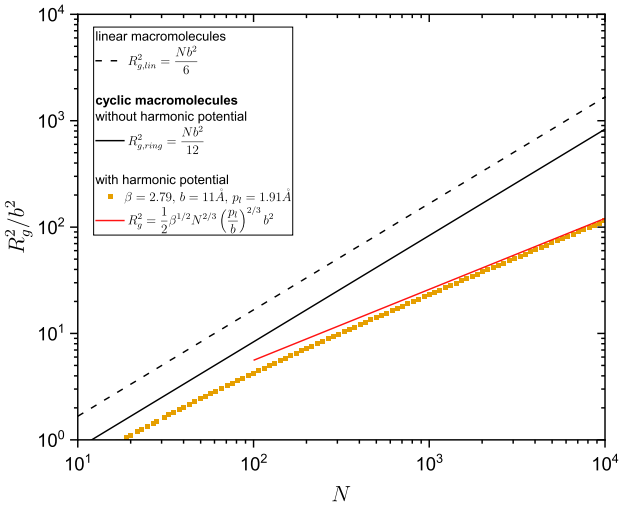

FIG. 4. In contrast to Fig. 1, this illustration of the mean squared radius of gyration now takes into account the relation between the characteristic radius $\tilde{R}$ of the potential and the number of Kuhn segments N as described in Eq. (32). The mean square radius of gyration no longer reaches a constant value at large N but rather approaches a $N^{2/3}$ dependence. The mean squared radius of gyration is normalized by the squared length b^2 of a Kuhn segment, and the following equation was used for its calculation: $R_g^2 = 2\frac{Nb^2}{4\pi^2}\sum_{p=1}^{N/2}\left(p^2 + \frac{1}{4\pi^2}\frac{N^{2/3}}{\beta}\left(\frac{b}{p_l}\right)^{4/3}\right)^{-1}$ with $\beta = \left(\frac{3}{\pi}\right)^2\left(\frac{\pi}{6}\right)^{2/3}\left(\frac{R_g}{\tilde{R}_{sf}}\right)^4 \approx 2.79$ using $R_g \approx 49.5$Å, $\tilde{R}_{sf} \approx 33.6$Å, $b = 11$Å, and $p_l = 1.91$Å obtained from the literature for polyethylene oxide.[10,11,20,26,27]

Another feature of the model is related to the fact that the attractive potential defined in Eq. (1) does not change the self-diffusion coefficient of the polymer ring but strongly shortens the terminal relaxation time compared to the Rouse relaxation time; see Eq. (12),

$$\tau_1 \cong \bar{\tau}_1 = \pi^2\frac{\tilde{R}^2}{b^2}\tau_s = 4\pi^2\frac{R_g^4}{b^4}\tau_s \ll \tau_R = \tau_s N^2. \tag{36}$$

At times of order τ_1, the MSD of the ring segments reaches the asymptotic value $2R_g^2 = \tilde{R}b$, while the MSD of the center of mass is even much smaller and begins to dominate only at much longer times $t \gg \bar{\tau}_1^* = \frac{\bar{\tau}_1}{4}\frac{Nb^2}{R_g^2} = 3\bar{\tau}_1\frac{R_{g,ideal}^2}{R_g^2}$; see Fig. 3. Taking into account expressions written above, for the potential defined in Eq. (33), one can find that $\frac{\bar{\tau}_1^*}{\tau_1} = \frac{1}{2\sqrt{\beta}}N^{1/3}\left(\frac{b}{p_l}\right)^{2/3}$. Effectively, this results in the transition to the normal diffusion regime being delayed for an extended time interval $\bar{\tau}_1 \le t \le \bar{\tau}_1^*$, in which the time dependence of the mean-squared displacement of the segments slows down toward a quasi-plateau for large N. An indication of the quasi-plateau on mean squared displacement has been recently observed by neutron spin echo spectroscopy performed on the fully hydrogenated sample

to observe a self-correlation function [Eq. (17)]. Interestingly, the crossover to the slower power law takes place at 13.5 ns, which, in terms of parameters for poly(ethylene oxide), corresponds to $10^3\ \tau_s$, i.e., about 10 ns.

At the end of this section, we show that Eq. (32), which defines the intensity of the harmonic potential, can be obtained based on scaling relations in the spirit of mean-field considerations of Flory. Consider the situation in which the radius of inertia of a polymer ring R is much smaller than its ideal dimensions, $R \ll b\sqrt{\frac{N}{12}}$. The equilibrium value of the radius of inertia R_g will be determined by a compromise of two opposing tendencies.

On one hand, entropic elasticity forces of the ring will try to increase R to the equilibrium value of the ideal ring. On the other hand, the forces associated with topological restrictions for neighboring polymer rings when crossing the contour of a given polymer ring will tend to reduce its linear dimensions to the smallest possible size. The probability density for a linear ideal polymer chain to have a given radius of gyration R is known (see, e.g., Ref. 17 and the literature cited therein). For the situation of strong compression, i.e., when $R^2 \ll \frac{Nb^2}{6}$, it is given in our notations by the following expression:

$$W_{el}^{lin}(R) = \frac{3}{\sqrt{6\pi}}\frac{1}{Nb^2}\left(\frac{Nb^2}{R^2}\right)^{5/2}\exp\left(-\frac{3}{8}\frac{Nb^2}{R^2}\right). \tag{37}$$

We repeated largely similar calculations for ideal ring macromolecules (see the Appendix), and the result for the case of strong compression, i.e., when $R^2 \ll \frac{Nb^2}{12}$, was as follows:

$$W_{el}^{ring}(R) = \frac{6}{\sqrt{2\pi}}\frac{1}{N^{1/2}b}\left(\frac{Nb^2}{R^2}\right)^{4}\exp\left(-\frac{3}{8}\frac{Nb^2}{R^2}\right). \tag{38}$$

As can be easily seen, relations (37) and (38) at N ≫ 1 differ insignificantly from each other under strong compression only by the pre-exponential coefficient, reflecting the difference in the architecture of linear and ring macromolecules.

The effective entropic energy of elasticity corresponding to the distribution Eq. (38) is given by the following expression:

$$U_{el}(R) = -k_BT\ \ln\ W_{el}^{ring}(R). \tag{39}$$

Omitting numerical multipliers and weak logarithmic additives, the following estimate can be made on the basis of relations (38) and (39):

$$U_{el}(R) \propto k_BT\frac{Nb^2}{R^2}. \tag{40}$$

Note that the pre-exponential coefficients of relations (37) and (38) lead only to logarithmically weak corrections in (39) and (40), which are negligible when N ≫ 1. An estimate of the effective energy associated with topological interactions of polymer rings located at least partially in the volume R^3 can be made as follows. In the volume R^3, there are $\rho_s R^3$ polymer segments. Assuming that $R \ll b\sqrt{\frac{N}{12}}$ and the polymer rings are ideal, each piece of the ring whose ends are separated by the distance R from each other, i.e., some kind of blob, contains an order of $n_b \propto \frac{R^2}{b^2}$ polymer segments. Thus, within the volume R^3 under consideration, there are on the order of $N_b(R) \propto \frac{\rho_s R^3}{n_b} = \rho_s b^2 R$ different blobs. Each such blob interferes with the penetration of polymer segments external to the volume under consideration for topological reasons. It is natural to assume that each blob contributes an amount on the order of k_BT to the repulsion energy of the external segments. Consequently, the energy associated with topological constraints can be naturally estimated as

$$U_{tp}(R) \propto k_BTN_b(R) = k_BT\rho_s b^2 R. \tag{41}$$

The total effective energy can then be estimated as

$$U^{eff}(R) = U_{el}(R) + U_{tp}(R). \tag{42}$$

The minimum of this energy, which is easily seen from relations (40) and (41), is reached at R_g of order

$$R_g \propto \rho_s^{-1/3}N^{1/3}. \tag{43}$$

Recalling [see Eq. (11)] that for the case under discussion $R_g^2 = \frac{1}{2}\tilde{R}b$, we see that Eq. (43) agrees with Eq. (32).

Note also that we completely ignored the presence of excluded volume segment–segment interactions, which is an acceptable approximation in accordance with the well-known Flory's near-ideality theorem for polymer melts. The behavior of polymer rings in good solvents, where excluded volume interactions become crucial, can be found in Ref. 28 and the literature cited therein. In dilute θ-solutions of cyclic macromolecules containing a sufficiently large number of Kuhn segments, $N > N_0 = 250 \ldots 300$ (see details in Refs. 29 and 30), there are possible interactions of excluded volume, induced by intramolecular topological prohibitions of the cyclic macromolecule, to form complex knots. This leads to the fact that sufficiently large cyclic macromolecules turn out to be swollen, i.e., to have dimensions substantially larger than ideal ones. In melts, this additional effect, as noted in Ref. 29, for large $N > N_0$ leads to the ratio (43) with an additional numerical multiplier $N_0^{1/6} \approx 2.6$. In our extremely simple formalism, which allows for a rather complete analytical analysis, this effect, if it proves to be significant, can at least phenomenologically be accounted for by means of the coefficient β in relation (32). Then the concentration of the intrinsic Kuhn segments $\tilde{\rho}_s(0)$ given by expression (29) at the center of mass of each globule formed by the compressed ring should depend on the molecular mass and, at large $N > N_0$, be approximately $N_0^{1/2} \approx 10 \ldots 15$ times less than the concentration of polymer segments of the melt. The computer experiments known to us do not reproduce such behavior. Moreover, the experimental data discussed above indicate a substantially larger concentration of its own segments in the center of the globule [see expression (31) and the text below]. However, this fact requires additional experimental and theoretical study.

IV. CONCLUSIONS

In this study, we investigate the dynamic behavior of non-concatenated polymer rings based on a simple model, the Rouse model modified by a spherical attractive harmonic potential. Despite significant simplifications, the model has important nontrivial properties.

The model shows a high sensitivity of the conformation of large polymer rings, i.e., consisting of a large number of Kuhn segments

$N \gg 1$, to the characteristic radius of the attractive potential, i.e., the potential strength. For sufficiently strong potentials, $\tilde{R} \ll \frac{Nb}{2\pi}$, the polymer rings experience a strong contraction in comparison with the ideal state, and their characteristic linear dimensions become much smaller than in ideal rings $R_g^2 = \frac{1}{2}\tilde{R}b \ll \frac{Nb^2}{12} = R_{g,ideal}^2$ (see Fig. 1). When taking into account the relation between the characteristic radius of the potential and the size of the macromolecules, $\tilde{R} \propto N^{4/3}$, the radius of gyration approaches the weakened molecular-mass dependence of $R_g^2 \propto N^{2/3}$ observed in computer simulations (Fig. 4).[6,7]

Furthermore, the time dependence of the mean squared displacement of the ring segments is slowed down in the time interval $\overline{\tau}_1 \le t \le \overline{\tau}_1^*$ and approaches a quasi-plateau at $2R_g^2 = \tilde{R}b$ for large N (see Fig. 3), effectively delaying the transition to the normal diffusion regime. Note that anomalous behavior in the normal diffusion regime in melts of cyclic macromolecules has been repeatedly observed in computer simulations[4,12] but has not yet been found experimentally. Probably, although simplified, this is already reflected in the discussed, strongly simplified, model. However, a more specific discussion of the latter aspect requires a more realistic description of the intramolecular and intermolecular entanglement effects than provided by the terms associated with the friction forces and the stochastic Langevin force in Eq. (3), for example, on the Mori–Zwanzig memory function formalism. Corresponding work is in progress.

AUTHOR DECLARATIONS

Conflict of Interest

The authors have no conflicts to disclose.

Author Contributions

Nail Fatkullin: Conceptualization (equal); Data curation (equal); Formal analysis (equal); Investigation (equal); Methodology (equal); Supervision (equal); Validation (equal); Visualization (equal); Writing – original draft (equal); Writing – review & editing (equal). **Carlos Mattea**: Conceptualization (equal); Data curation (equal); Formal analysis (equal); Investigation (equal); Methodology (equal); Validation (equal); Visualization (equal); Writing – original draft (equal); Writing – review & editing (equal). **Kevin Lindt**: Data curation (equal); Formal analysis (equal); Investigation (equal); Validation (equal); Visualization (equal); Writing – original draft (equal); Writing – review & editing (equal). **Siegfried Stapf**: Conceptualization (equal); Data curation (equal); Formal analysis (equal); Investigation (equal); Validation (equal); Visualization (equal); Writing – original draft (equal); Writing – review & editing (equal). **Margarita Kruteva**: Conceptualization (equal); Formal analysis (equal); Investigation (equal); Supervision (equal); Validation (equal); Visualization (equal); Writing – original draft (equal); Writing – review & editing (equal).

DATA AVAILABILITY

No data from experiments or simulations were presented in this study. The data presented in Figs. 1–4 were generated by examining the corresponding equations using Python 3.13.1 and visualized with OriginPro 2022. The Python scripts are available on Zenodo, https://doi.org/10.5281/zenodo.14956318.

APPENDIX: THE GYRATION RADIUS DISTRIBUTION FUNCTION FOR IDEAL RING MACROMOLECULES

Let us consider the square of the radius of inertia of a cyclic ideal macromolecule. It can be expressed as follows through the normal modes of Rouse:

$$S^2 \equiv \frac{1}{N}\sum_n (\vec{r}_n - \vec{r}_{cm})^2 = 2\sum_{p=1,2\ldots N/2} \left(\vec{X}_p^2 + \vec{Y}_p^2\right). \tag{A1}$$

It is convenient to begin the calculations by considering the distribution function of the square of the radius of inertia,

$$\tilde{W}\left(R^2\right) \equiv \left\langle \delta\left(R^2 - S^2\right)\right\rangle, \tag{A2}$$

where the parentheses $\langle\cdots\rangle$ denote the equilibrium averaging over all conformations of an ideal cyclic macromolecule or, equivalently, over the distribution of Rouse normal modes $\vec{X}_p$, $\vec{Y}_p$.

The inertia radius distribution function $W(R)$ is related to $\tilde{W}\left(R^2\right)$ by the following relationship:

$$W(R) = 2R\tilde{W}\left(R^2\right). \tag{A3}$$

Next, we note that the normal modes of Rouse for an ideal ring macromolecule have a Gaussian distribution, and their root mean square values satisfy the relation

$$\left\langle \vec{X}_p^2\right\rangle_{eq} = \left\langle \vec{Y}_p^2\right\rangle_{eq} = \frac{Nb^2}{8\pi^2p^2} = \frac{3}{2}\frac{R_g^2}{\pi^2p^2}. \tag{A4}$$

Using the Fourier representation for the Dirac function and the independence of the distribution of various normal modes of Rouse, we transform the ratio (A2) as follows:

$$\begin{aligned}
\tilde{W}\left(R^2\right) \equiv \left\langle \delta\left(R^2 - S^2\right)\right\rangle &= \int_{-\infty}^{+\infty}\frac{d\kappa}{2\pi}\left\langle \exp\left\{i\kappa\left(R^2 - S^2\right)\right\}\right\rangle \\
&= \int_{-\infty}^{+\infty}\frac{d\kappa}{2\pi}\exp\left\{i\kappa R^2\right\}\left\langle \exp\left\{-i\kappa S^2\right\}\right\rangle \\
&= \int_{-\infty}^{+\infty}\frac{d\kappa}{2\pi}\exp\left\{i\kappa R^2\right\}\left\langle \exp\left\{-i2\kappa\sum_{p=1,\ldots N/2}\left(X_p^2 + Y_p^2\right)\right\}\right\rangle \\
&= \int_{-\infty}^{+\infty}\frac{d\kappa}{2\pi}\exp\left\{i\kappa R^2\right\}\prod_{p=1,\ldots N/2}\left\langle \exp\left\{-i2\kappa\left(X_p^2 + Y_p^2\right)\right\}\right\rangle \\
&= \int_{-\infty}^{+\infty}\frac{d\kappa}{2\pi}\exp\left\{i\kappa R^2\right\}\prod_{p=1,\ldots N/2}\left(1 + \frac{4i\kappa}{3}\left\langle X_p^2\right\rangle\right)^{-3}.
\end{aligned} \tag{A5}$$

For large N $\gg$ 1, the approximation can be used,

$$\prod_{p=1}^{N/2}\left(1 - \frac{Z^2}{\pi^2p^2}\right) \approx \prod_{p=1}^{\infty}\left(1 - \frac{Z^2}{\pi^2p^2}\right) = \frac{\sin(Z)}{Z}. \tag{A6}$$

This approximation allows ratio (A5) to be rewritten as follows:

$$\tilde{W}\left(R^2\right) = \int_{-\infty}^{+\infty}\frac{d\kappa}{2\pi}\exp\left\{i\kappa R^2\right\}\left(\frac{Z}{\sin Z}\right)^3 \tag{A7}$$

with $Z^2 = \frac{2}{i}R_g^2\kappa$.

For the distribution function of the radius of inertia, the following relationship can be obtained:

$$W(R) = 2R\tilde{W}\left(R^2\right) = 2R\int_{-\infty}^{+\infty}\frac{d\kappa}{2\pi}\left[\frac{Z}{\sin Z}\right]^3 \exp\left\{i\kappa R^2\right\}$$
$$= 2R\int_{-\infty}^{+\infty}\frac{d\kappa}{2\pi}\left[\frac{Z}{\frac{e^{iZ}+e^{-iZ}}{2i}}\right]^3 = \frac{(2i)^3 R}{\pi}\int_{-\infty}^{+\infty} d\kappa\left[\frac{Z}{1-e^{-2iZ}}\right]^3 \exp\left\{i\kappa R^2 - 3iZ\right\}$$
$$= \frac{(2i)^3 i}{\pi}\frac{R}{R_g^2}\int_{-\infty}^{+\infty}\left[\frac{1}{1-e^{-2iZ}}\right]^3 Z^4 \exp\left\{-\frac{1}{2}Z^2 t - 3iZ\right\}dZ, \tag{A8}$$

with $t = \frac{R^2}{R_g^2}$.

Using for $t \ll 1$ the method of steepest descents for evaluating the integral on the left side of the last line in relation (A8), one can obtain

$$W(R) = \frac{8\cdot 3^4}{\sqrt{2\pi}}\frac{t^{-4}}{R_g}\exp\left(-\frac{9}{2t}\right) = \frac{6}{\sqrt{2\pi}}\frac{1}{N^{1/2}b} \times\left(\frac{Nb^2}{R^2}\right)^4 \exp\left(-\frac{3}{8}\frac{Nb^2}{R^2}\right). \tag{A9}$$

Note that the exponential factor of this expression is identical to the corresponding exponential factor of the distribution function of gyration radius for linear chains at a similar limit; see Refs. 17, 31, and 32.

In the opposite limit, $t \gg 1$, we should return to the following representation:

$$W(R) = 2R\int_{-\infty}^{+\infty}\frac{d\kappa}{2\pi}\exp\left\{i\kappa R^2\right\}\prod_{p=1,\ldots N/2}\left(1+\frac{4i\kappa}{3}\left\langle\vec{X}_p^2\right\rangle\right)^{-3}$$
$$= 2R\int_{-\infty}^{+\infty}\frac{d\kappa}{2\pi}\exp\left\{i\kappa R^2\right\}\prod_{p=1,\ldots N/2}\left(\frac{1}{1+\frac{4i\kappa}{3}\left\langle\vec{X}_p^2\right\rangle}\right)^3. \tag{A10}$$

When

$$\kappa = \kappa_p = \frac{3i}{4\left\langle\vec{X}_p^2\right\rangle}, \tag{A11}$$

the integrable function has poles of the third order at the imaginary axis.

By a suitable choice of the integration contour and approximation (A6), we can represent the required integral as a sum of contributions from the poles,

$$W(R) = 2R\sum_q\int_{C_q}\frac{d\kappa}{2\pi}\exp\left\{i\kappa R^2\right\}\prod_{p=1,\ldots N/2}\left(\frac{1}{1+\frac{4i\kappa}{3}\left\langle\vec{X}_p^2\right\rangle}\right)^3$$
$$= 2R\sum_q\int_{C_q}\frac{d\kappa}{2\pi}\exp\left\{i\kappa R^2\right\} \times\left(\frac{Z\left(1+\frac{4i\kappa}{3}\left\langle\vec{X}_q^2\right\rangle\right)}{\sin Z}\right)^3\left(\frac{3}{4i\left\langle X_q^2\right\rangle}\frac{1}{\kappa-\kappa_q}\right)^3, \tag{A12}$$

where $\kappa_p = \frac{3i}{4\left\langle\vec{X}_p^2\right\rangle}$.

Then, calculations can be performed according to the following procedure:

$$W(R) = 2R\sum_q\int_{C_q}\frac{d\kappa}{2\pi}\exp\left\{i\kappa R^2\right\} \times\left(\frac{Z\left(1+\frac{4i\kappa}{3}\left\langle\vec{X}_q^2\right\rangle\right)}{\sin Z}\right)^3\left(\frac{3}{4i\left\langle X_q^2\right\rangle}\frac{1}{\kappa-\kappa_q}\right)^3$$
$$= -R\sum_q\left(\frac{3}{4\left\langle X_q^2\right\rangle}\right)^3 \times\frac{\partial^2}{\partial\kappa^2}\left(\exp\left\{i\kappa R^2\right\}\left(\frac{Z\left(1+\frac{4i\kappa}{3}\left\langle X_q^2\right\rangle\right)}{\sin Z}\right)^3_{\kappa\to\kappa_q}\right)_{\kappa=\kappa_q}. \tag{A13}$$

The leading contribution when considering the limit $t \gg 1$ is as follows:

$$W(R) = R^5\left(\frac{3}{4\left\langle X_1^2\right\rangle}\right)^3\exp\left\{i\kappa_1 R^2\right\}\left(\frac{Z\left(1+\frac{4i\kappa}{3}\left\langle X_1^2\right\rangle\right)}{\sin Z}\right)^3_{\kappa\to\kappa_1}$$
$$= \pi^3\frac{t^{2.5}}{R_g}\exp\left(-\frac{\pi^2}{8}t\right). \tag{A14}$$

Note that the exponential factor in this limit, as in the ratio (A9), is the same as the corresponding expressions for ideal linear macromolecules. Differences in the architecture of linear and ring macromolecules are reflected only in the pre-exponential factors; see Refs. 17, 31, and 32.

REFERENCES

[1] M. Rubinstein, Phys. Rev. Lett. **57**, 3023–3026 (1986).
[2] M. Kruteva, J. Allgaier, and D. Richter, Macromolecules **56**, 7203–7229 (2023).
[3] T. Ge, S. Panyukov, and M. Rubinstein, Macromolecules **49**, 708–722 (2016).
[4] Z. E. Dell and K. S. Schweizer, Soft Matter **14**, 9132–9142 (2018).
[5] B. Mei, Z. E. Dell, and K. S. Schweizer, Macromolecules **53**, 10431–10445 (2020).
[6] J. D. Halverson, W. B. Lee, G. S. Grest, A. Y. Grosberg, and K. Kremer, J. Chem. Phys. **134**, 204904 (2011).
[7] J. D. Halverson, W. B. Lee, G. S. Grest, A. Y. Grosberg, and K. Kremer, J. Chem. Phys. **134**, 204905 (2011).
[8] D. G. Tsalikis, V. G. Mavrantzas, and D. Vlassopoulos, ACS Macro Lett. **5**, 755–760 (2016).
[9] M. Kruteva, J. Allgaier, M. Monkenbusch, L. Porcar, and D. Richter, ACS Macro Lett. **9**, 507–511 (2020).
[10] M. Kruteva, M. Monkenbusch, J. Allgaier, O. Holderer, S. Pasini, I. Hoffmann, and D. Richter, Phys. Rev. Lett. **125**, 238004 (2020).
[11] M. Kruteva, J. Allgaier, M. Monkenbusch, I. Hoffmann, and D. Richter, J. Rheol. **65**, 713–727 (2021).

[12] J. D. Halverson, K. Kremer, and A. Y. Grosberg, J. Phys. A: Math. Theor. **46**, 065002 (2013).
[13] R. Pasquino, T. C. Vasilakopoulos, Y. C. Jeong, H. Lee, S. Rogers, G. Sakellariou, J. Allgaier, A. Takano, A. R. Brás, T. Chang, S. Goußen, W. Pyckhout-Hintzen, A. Wischnewski, N. Hadjichristidis, D. Richter, M. Rubinstein, and D. Vlassopoulos, ACS Macro Lett. **2**, 874–878 (2013).
[14] M. Q. Tu, O. Davydovich, B. Mei, P. K. Singh, G. S. Grest, K. S. Schweizer, T. C. O'Connor, and C. M. Schroeder, ACS Polym. Au **3**, 307–317 (2023).
[15] K. L. Ngai, J. Polym. Sci. **62**, 174–181 (2024).
[16] S. Goto, K. Kim, and N. Matubayasi, J. Chem. Phys. **155**, 124901 (2021).
[17] H. Yamakawa, *Modern Theory of Polymer Solutions* (Harper & Row, 1971).
[18] M. Doi and S. F. Edwards, *The Theory of Polymer Dynamics* (Oxford University Press, 1988).
[19] A. Y. Grosberg and A. R. Khokhlov, *Statistical Physics of Macromolecules* (AIP Press, 1994).
[20] M. Rubinstein and R. H. Colby, *Polymer Physics* (Oxford University Press, 2003).
[21] P. G. de Gennes, *Scaling Concepts in Polymer Physics* (Cornell University Press, 1979).
[22] G. R. Strobl, *The Physics of Polymers* (Springer, 1997).
[23] A. Denissov, M. Kroutieva, N. Fatkullin, and R. Kimmich, J. Chem. Phys. **116**, 5217 (2002).
[24] M. Dolgushev and M. Krutyeva, Macromol. Theory Simul. **21**, 565–572 (2012).
[25] X. Tian, J. Chen, Z.-C. Yan, W.-S. Xu, T. Shi, and D. Wang, Macromolecules **58**(9), 4500–4508 (2025).
[26] K. Lindt, N. Fatkullin, C. Mattea, J. Allgaier, S. Stapf, and M. Kruteva, Macromolecules **57**(8), 3765 (2024).
[27] L. J. Fetters, D. J. Lohse, D. Richter, T. A. Witten, and A. Zirkel in *Physical Properties of Polymers Handbook*, edited by J. E. Mark (Springer, 2007), Chap. 25.
[28] M. Handa and P. Biswasa, J. Rheol. **65**(4), 595–604 (2021).
[29] A. Y. Grosberg, Phys. Rev. Lett. **85**, 3858 (2000).
[30] A. Y. Grosberg, Polym. Sci., Ser. A **51**(1), 70–79 (2009).
[31] M. Fixman, J. Chem. Phys. **36**, 306–310 (1962).
[32] W. C. Forsman, J. Chem. Phys. **42**, 2829–2835 (1965).